



Assessment of the physicochemical properties of chrysotile-containing brake debris pertaining to toxicity

Matthew S. P. Boyles, Craig A. Poland, Jennifer Raftis & Rodger Duffin

To cite this article: Matthew S. P. Boyles, Craig A. Poland, Jennifer Raftis & Rodger Duffin (2019) Assessment of the physicochemical properties of chrysotile-containing brake debris pertaining to toxicity, *Inhalation Toxicology*, 31:8, 325-342, DOI: [10.1080/08958378.2019.1683103](https://doi.org/10.1080/08958378.2019.1683103)

To link to this article: <https://doi.org/10.1080/08958378.2019.1683103>



© 2019 The Author(s). Published by Informa UK Limited, trading as Taylor & Francis Group.



[View supplementary material](#)



Published online: 05 Nov 2019.



[Submit your article to this journal](#)



Article views: 1554



[View related articles](#)



[View Crossmark data](#)



Citing articles: 5 [View citing articles](#)

Assessment of the physicochemical properties of chrysotile-containing brake debris pertaining to toxicity

Matthew S. P. Boyles^{a*}, Craig A. Poland^{b*}, Jennifer Raftis^b and Rodger Duffin^{b,c}

^aInstitute of Occupational Medicine, Research Avenue North, Edinburgh, UK; ^bCentre for Inflammation Research, Queen's Medical Research Institute, The University of Edinburgh, Edinburgh, UK; ^cConcept Life Sciences, 2 James Lindsay Place Dundee Technopole Dundee, Dundee, Scotland

ABSTRACT

Grinding and drilling of chrysotile asbestos-containing brake pads during the 20th century led to release of chrysotile, resulting in varying levels of workplace exposures of mechanics. Despite exposures, excess risk of mesothelioma remains in doubt.

Objectives: The toxicity of particulates is primarily derived through a combination of physicochemical properties and dose and as such this study aimed to determine properties of asbestos-containing brake debris (BD) which may influence pathogenicity and potential of mesothelioma.

Materials and Methods: Chrysotile-containing brake pads were ground – to reflect occupational activities, aerosolized, and size-fractionated to isolate respirable fractions. Analysis of morphology, biodurability, surface charge, and interactions with macrophages were undertaken.

Results: The respirable fraction of BD contained ~15–17% free chrysotile fibers thereby constituting a small but relevant potential long fiber dose. Acellular biodurability studies showed rapid dissolution and fragmentation of chrysotile fibers that was consistent for pure chrysotile control and BD samples.

Conclusions: The long, free, respirable chrysotile fibers were present in BD, yet were of low bio-durability; incubation in artificial lysosomal fluid led to destruction of free fibers.

ARTICLE HISTORY

Received 9 May 2019
Accepted 17 October 2019

KEYWORDS



Brake debris; chrysotile asbestos; fiber; toxicity; mesothelioma

Introduction

The use of chrysotile in commercial products has a long history and exposure to these 'asbestos' fibers during chrysotile production, goods manufacture, or use of chrysotile containing products has led to varying incidences of disease (Becklake et al. 2007). One such example of the use of chrysotile and subsequent worker exposure is friction materials such as brake and clutch pads for the automotive and aviation industry. Brake pads which generally consist of five main elements: binders, fibers, fillers, frictional additives, and abrasives (Grigoratos and Martini 2015). The use of chrysotile fibers was to provide mechanical strength and accounted for as much as 50% of the brake composition by mass (Lynch 1968; Weir and Meraz 2001). In the fitting of brake pads, machining (e.g. grinding, drilling) was typically an integral part of achieving an effective fit and contact during the mounting of brake pads. Grinding of a composite can result in the release of respirable debris comprising the constituents of the composite, in this case phenolic resins, carbon, and chrysotile in various bound and unbound forms. Workers undertaking such activities are exposed to the dust generated during machining and research has

shown the release of chrysotile fragments and fibers (see Paustenbach et al. 2003; Paustenbach et al. 2004; Kelsh et al. 2007 for a comprehensive review). Unsurprisingly, due to the wide variety of work environments, practices, vehicle types and frequency of brake repair, exposure levels among auto-mechanics varies considerably. Larger exposure studies have shown low cumulative levels of chrysotile exposure, below that which may be attained at the Occupational Safety and Health Administration Permissible Exposure Limit (PEL) of 0.1 f/cm³ (Paustenbach et al. 2003; Finley et al. 2007). However, other studies have shown exposures that exceed such limits in Bogotá, Columbia (Salazar et al. 2015), Europe (Rodelsperger et al. 1986; Gustavsson et al. 1990) as well as the US (Rohl et al. 1976) indicating unsafe work practices and possible excess risk of 'asbestos'-related disease.

While 'asbestos' has been proven to be a causal factor in a litany of fibrotic and tumorigenic diseases, malignant mesothelioma (MM) is perhaps the most specific as, with rare exception, it is predominantly associated with past 'asbestos' exposure. As such, it would be expected that such a documented exposure may lead to an excess risk of MM. However, numerous epidemiological studies have yet to

CONTACT Rodger Duffin  Rodger.Duffin@ed.ac.uk  Centre for Inflammation Research, Queen's Medical Research Institute, The University of Edinburgh, 47 Little France Crescent, Edinburgh, EH16 4TJ, UK

*These authors contributed equally to this work.

 Supplemental data for this article can be accessed at <https://doi.org/10.1080/08958378.2019.1683103>.

© 2019 The Author(s). Published by Informa UK Limited, trading as Taylor & Francis Group.

This is an Open Access article distributed under the terms of the Creative Commons Attribution-NonCommercial-NoDerivatives License (<http://creativecommons.org/licenses/by-nc-nd/4.0/>), which permits non-commercial re-use, distribution, and reproduction in any medium, provided the original work is properly cited, and is not altered, transformed, or built upon in any way.

demonstrate an excess risk of 'asbestos'-related disease including MM within this exposure cohort (Wong 2001; Goodman et al. 2004; Laden et al. 2004; Garabrant et al. 2016). It is important to note however that such epidemiological conclusions are not universally shared (Egilman and Billings 2005) and furthermore, there are case studies describing MM in auto mechanics working with chrysotile containing friction products (Langer and McCaughey 1982; Finkelstein 2015). For further discussion of the literature, refer to Poland and Duffin (2019).

Chrysotile asbestos together with amphiboles such as crocidolite, tremolite, and amosite are all Class 1 carcinogens (IARC 2012). Yet the debris released from chrysotile containing brake products contains what may be considered adulterated chrysotile owing to the (a) incorporation into a resin matrix, (b) pressure and heat curing, (c) high shear stress during grinding, and (d) heat due to grinding friction. It is therefore certainly plausible that such conditions could modify the morphological as well as physicochemical characteristics of the chrysotile released from the resin matrix (Poland and Duffin 2019).

In relation to particle and fiber toxicology, the relative risk of (any) disease related to a particulate is determined by the dose (as dictated by the exposure characteristics) as well as the morphological and physicochemical characteristics of a particle/fiber. In terms of chrysotile containing brake debris (BD), the exposure of workers has been shown and as such, a possible reason behind a lack of excess risk may lie in the morphological and physicochemical characteristics of the released material. This study seeks to understand the key properties of asbestos BD, derived from grinding of asbestos brake pads that may influence the human toxicity of the contained asbestos fibers.

Methods

Sample preparation

Three samples of BD, identified as *BD-A*, *BD-B*, and *BD-C* were generated directly from chrysotile-containing automotive drum brake shoes by the RJ Lee Group Ltd. (Monroeville, PA). As described by Bernstein et al. (2014), the brake shoes were ground using a commercial AMMCO arc grinder (Model 8000, S/N 24788) with an attached quartz micro-fiber filter and Tisch high volume air sampler sampling pump (Tisch Environmental Inc., Ohio, USA). The size and shape of this bulk material was highly heterogeneous and so separation of a respirable fraction was performed through aerosolization of each sample in an aerosolization chamber (Aero PA100, Model NA002, Naneum, Canterbury, UK) as described by Ding et al. (2015). The chamber generates an aerosol from bulk sample by applying high velocity air jets to the powder surface. After passing through a HEPA filter, dry clean air is driven through a nozzle with three small holes to create high velocity jets for aerosolization. The flow rate for the jets was set at 5 L/min after which the aerosol passes through a 11.5-cm diameter, 10 L polypropylene bottle as a classification chamber. Within the classification chamber, particles,

and particle agglomerates were separated as a function of particle diameter, density, and air flow (Stokes Law). Charge neutralization was not employed within the aerosolization and gravitational separation procedure. Particles were aerosolized 'as received' were not subject to further grinding or other preparatory methods prior to aerosolization.

After gravitational separation, particles were collected with a respirable filter head (25 mm Higgins Dewell Cyclone, SKC, Dorset, UK). The collection efficiency curve of the respirable head met the ACHIH/ISO/CEN standards (EN481) for a respirable curve with a median 50% cut point of 4 μm (aerodynamic equivalent diameter). The size distribution of the obtained respirable fractions was confirmed using an aerodynamic particle sizer (APS) 3321 spectrometer (TSI Incorporated, Minnesota, USA) and DustTrak DRX Aerosol Monitor 8533 (TSI Incorporated, Minnesota, USA), following manufactures procedure.

In addition to the BD samples, UICC B chrysotile asbestos (*UICC-Chry-B*) was used as a pure chrysotile comparator, UICC amosite asbestos was used as a biodurable amphibole and MMVF10 as a bio-soluble glass fiber.

Incubation in biofluid

All test materials were suspended in quadruplicate in an artificial lysosomal fluid (ALF; used to simulate the phagolysosome compartment of alveolar macrophages) at 0.3 mg/ml and incubated in a static system at 37 °C for 0, 1, 2, 3, 7, 14, 42, 84, 126, and 168 days. After this incubation period, samples were isolated via vacuum filtration onto 47 mm polycarbonate filters with a pore size of 0.2 μm . The effluent was kept for inductively coupled plasma optical emission spectrometry (ICP-OES) analysis of dissolved elements and the material residue was dried, quadruplicates pooled, and aliquots of each prepared for subsequent characterization. The ALF used was based on that previously reported by Marques et al. (2011) (see [Supplementary Methods](#) for composition).

Characterization

Particulate dissolution

The dissolution of each material was established by two methods. First, gravimetric analysis was performed by assessing weights of the dried residual material collected pre-weighed polycarbonate filters ($n = 4$). Second, the quantity of leached silicon, magnesium, and iron in the filtered solution were determined by ICP-OES using an iCAP 6000 series (Thermo Scientific) (four replicates pooled). Prior to analysis by ICP-OES, each sample was digested using nitric, hydrochloric, and hydrofluoric acids, with 30% hydrogen peroxide solution in Teflon type beakers on a hotplate. In a static dissolution system, the monitoring of changes in overall mass remaining, or chemical changes of incubation fluid, allow for a limited assessment of dissolution rates (Searl et al. 1999). Therefore, the data from particles dissolution are presented as mass retention, mass loss per hour of

exposure time, concentration of solutes detected in incubation fluid, and Si leached per hour of incubation time.

Surface charge

The surface charge of all materials was determined by measuring zeta potential using a Malvern NanoZS (Malvern Panalytical, Malvern, UK). Samples were suspended at 50 µg/ml in sodium chloride, which had previously been pH adjusted to pH 3, 5, 7, or 9 using either NaOH (1 M) or HCL (1 M) ($n = 3$ technical replicates, of four pooled samples). Data analysis and QC procedures were followed as per the ISO 13099 standard.

Reactive oxygen species analysis

Electron paramagnetic resonance (EPR) was used to measure superoxide radical generation from the surface of all materials used in this study using the spin trap 1-hydroxyl-2,2,6,6-tetramethyl-4-oxo-piperidine (Tempone-H) (see Supplementary methods for further details).

Scanning electron microscopy (SEM) and energy-dispersive X-ray spectroscopy (EDX)

SEM analysis was performed following an adaptation of International Organization for Standardization (ISO, 2002) 'Ambient Air – Determination of numerical concentration of inorganic fibrous particles – Scanning electron microscopy method.' The purpose was to assess and quantify morphological properties of the BD samples over time when incubated in ALF. Each sample was suspended in dH₂O and filtered through a 25 mm, 0.2 µm pore size polycarbonate filters. An excised portion of each filter was mounted on a 13 mm aluminum stub and sputter-coated with gold prior to examination. In addition to general morphological observations and elemental analysis, various structures were identified and quantified. These included particles with and without embedded fibers, 'free' World Health Organisation (WHO)-defined respirable fibers (with an aspect ratio >3:1, length >5 µm, and diameter <3 µm) (WHO 1997), and 'free' non-WHO-defined fibers. The classification of 'free' was based on the absence of any particle (e.g. resin) attachments to the chrysotile.

Owing to the mixed matrix, ground nature of the sample the number of 'free' fibers often comprised a sub-fraction of the total number of entities present in the prepared samples at each timepoint. In the isolated respirable fraction, 331, 223, and 348 'free' fibers were counted in samples A, B, and C, respectively, and then further sub-classified based on the above WHO definition. However, during the course of the study a considerable rate of dissolution occurred for some samples, and therefore there was a concomitant loss of fibers. As such, in a number of cases it was not possible to count a sufficient number of 'free' fibers. Where only a low number of fiber counts have been possible (i.e. below 100), the robustness of these data and potential restrictions should be considered when interpretation of size distributions is made. Within the fiber length distribution analysis, the total

number of measured fibers were sub-divided into size bins of <5, 5–10, 10–15, 15–20, 20–30, 30–40, 40–50, and 50+. A split procedure was not used with fibers counted only in their relative proportions.

Transmission electron microscopy (TEM)

TEM was used to further assess morphological changes of the BD samples which may have occurred during the incubation in ALF over time. Each sample was suspended in distilled water at 50 and 500 µg/ml and added to TEM grids prior to imaging using a JEOL JEM-1400 Plus transmission electron microscope. In addition to general morphological observations, BD were assessed for the occurrence of matrix particles alone, matrix containing fibers, and 'free' fibers.

Crystal structure

The structure of all materials was determined by X-ray diffraction (XRD). Each sample was ground to achieve a relatively uniform particle size prior to performing XRD techniques using a Bruker D2 Phaser X-ray diffractometer, operating with a 1D linear linxeye detector and generating copper K α radiation. Data were processed on the DQuant 1 software. XRD was only performed on the pristine samples as the mass remaining after biofluid incubation was not sufficient to perform this test.

Cell treatments

Cell culture

THP-1 cells were purchased from ATCC and were maintained at sub-culture in Roswell Park Memorial Institute 1640 Medium with glutamine (Lonza, UK) containing 10% heat inactivated fetal calf serum (Sigma-Aldrich, Poole, UK) and 50 units/mL penicillin and 50 µg/ml streptomycin (Sigma-Aldrich, Poole, UK). The cells were used between passages 4 and 15. Prior to cell treatments, the immature monocytic THP-1 cells in suspension culture (i.e. non-adherent) were differentiated into macrophage-type cells using 10 ng/ml of phorbol 12-myristate 13-acetate (PMA) in DMSO.

For electron microscopy analysis, Thermanox coverslips (Nunc) were placed into 24-well plates (Costar, UK) and the cells were seeded at a density of 0.5×10^6 /ml in 500 µl of culture media supplemented with 10 ng/ml of PMA. For cytocentrifugation preparations, cells were seeded into 25cm² cell culture flasks (Corning, UK) at a concentration of 0.5×10^6 /ml in 6.6 ml of culture media supplemented with 10 ng/ml of PMA. The cells were then cultured for 2 days at 37 °C in 5% CO₂. The use of these concentrations and volumes means that the cell density (0.132×10^6 /cm²) and media volume (263 µl/cm²) per unit surface area is the same in the 24-well plates and T25 culture flasks for total comparability during cell treatments. Cells were judged to be suitably differentiated when they were no longer in suspension and had fully adhered to the base of the well/flask.

Cytotoxicity analysis

Differentiated THP-1 cells in 24-well plates were washed with PBS to remove nonadherent cells. Cells were treated with respirable BD samples A, C, or UICC-Chry-B Asbestos at a range of concentrations consisting of 0, 1.25, 2.5, 5, 10, and 20 $\mu\text{g}/\text{cm}^2$ diluted from a stock concentration of 1 mg/ml before being vortex mixed and sonicated using a water bath sonicator at ambient temperature (frequency 50/60 Hz, power 28 W, Fisherbrand). After 24 h, the medium was removed and centrifuged at 2000 rpm for 5 min, transferred to a fresh tube and the supernatant centrifuged at 13 000 rpm for 5 min; cleared lysates were stored at 2–8 °C prior to the LDH assay (Roche, UK). Cytotoxicity was assessed using the LDH assay according to the manufacturers' specifications. For the LDH assay, the positive control Triton X-100 was added to the medium at 0.1% (v/v) and results were expressed as a percentage of maximal cell death. Sample BD-B was not assessed due to insufficient respirable sample.

Microscopy analysis

Differentiated THP-1 cells were treated with BD or UICC-Chry-B at a non-cytotoxic treatment dose of 2.5 $\mu\text{g}/\text{cm}^2$ (9.5 $\mu\text{g}/\text{ml}$) which was the same for treatments in both 24-well plates and T25 cell culture flasks for a period of 24 h at 37 °C in 5% CO_2 . The vehicle control was the culture media supplemented with 0.5% BSA with no particulates.

Electron microscopy. At the cessation of the treatment time, culture supernatant was removed and the cells washed gently with 500 μl of cold Dulbecco's phosphate buffered saline (Lonza, UK). Five hundred microliters of 2.5% glutaraldehyde in 0.1 M cacodylate buffer (Sigma Aldrich, Poole, UK) were then added to each well and refrigerated overnight. Dehydration and mounting procedures can be found in the supplementary methods.

Cyocentrifuge (Cytospin) preparations. At the end of the treatment period, the media supernatant was removed and the cells detached using 2 ml of 0.25% trypsin and 0.02% EDTA (Sigma-Aldrich, Poole, UK). The cell suspensions were centrifuged at 600 g for 5 min, the supernatant discarded and the cells re-suspended in 2 ml of Dulbecco's phosphate-buffered saline supplemented with 0.5% BSA.

The cell number of each treatment was determined via Trypan blue exclusion and 40 000 cells added to pre-prepared cyocentrifuge funnels and subjected to centrifugation at 300 rpm for 5 min. The cells on the glass slides were then fixed in 100% methanol and stained using hematoxylin and eosin (H&E) stain. Using optical microscopy, the proportion of cells with (i) no particles/fibers, (ii) internalized particles/fibers (complete uptake), or (iii) incomplete uptake of particles/fibers (indicative of frustrated phagocytosis) was determined by counting of a minimum of 600 cells per replicate.

Statistical analysis

The statistical analysis of EPR and gravimetric analysis data was performed with SPSS, using Kruskal–Wallis one-way analysis of variance (ANOVA) with all pairwise comparison, as data not found to be normally distributed. Statistical significance is given with a 95% confidence interval, i.e. when p value ≤ 0.05 . Cytotoxicity of the test particles was assessed with a one-way ANOVA using GraphPad Prism version 6 (GraphPad Software, La Jolla, CA).

Results

Characterization of respirable material

The bulk BD dust was highly heterogenous, with approximately 1/3 of the particulates showing no evidence of chrysotile (i.e. matrix particles) while the rest showed surface bound chrysotile (~30%) or unbound 'free' chrysotile (~40%). Similar proportions of matrix particles (no chrysotile) to chrysotile, either surface bound or 'free' were observed in the isolated respirable fractions. A full breakdown is provided in Tables S1–S3.

Aerosol properties

The respirable fraction of each BD sample was assessed by APC and DustTrak to identify that isolation was successful and to obtain data allowing the prediction of lung deposition. See Table 1 for summary aerosol characteristics and Figure S1 for APS size distribution analysis. The assessment of BD samples by APS provided a particle size distribution (PSD) based on aerodynamic diameter, while the DustTrak provided a mass of material within assigned size fractions. BD-A was shown to have a mono-modal number

Table 1. Particle aerodynamic diameters and size distributions of asbestos-containing BD samples with the aerosolisation of the respirable fractions, determined with Aerodynamic Particle Sizer Spectrometer and DustTrak DRX.

| | Respirable fraction | | |
|---|---------------------|-------|-------|
| | BD-A | BD-B | BD-C |
| Aerosolized respirable fraction: number-rated PSD (APS) | | | |
| Median (μm) | 1.13 | 1.34 | 1.21 |
| Mode (μm) | 0.898 | 0.898 | 0.898 |
| Geo. mean (μm) | 1.20 | 1.37 | 1.27 |
| Mean (μm) | 1.37 | 1.57 | 1.43 |
| Geo std dev (μm) | 1.63 | 1.68 | 1.62 |
| Aerosolized respirable fraction: mass-rated PSD (APS, calculated) | | | |
| Median (μm) (MMAD) | 2.16 | 2.48 | 2.77 |
| Mode (μm) | 2.13 | 2.84 | 2.64 |
| Geo. mean (μm) | 2.17 | 2.41 | 2.79 |
| Mean (μm) | 2.58 | 2.73 | 3.20 |
| Geo std dev (μm) | 1.79 | 1.68 | 1.68 |
| Aerosolized respirable fraction: surface area-rated PSD (APS, calculated) | | | |
| Median (μm) | 3.00 | 3.13 | 2.18 |
| Mode (μm) | 2.84 | 3.05 | 2.29 |
| Geo. mean (μm) | 3.78 | 3.09 | 2.13 |
| Mean (μm) | 3.11 | 3.44 | 2.44 |
| Geo std dev (μm) | 1.85 | 1.61 | 1.68 |
| Aerosolized respirable fraction: DustTrak size fractions (%) | | | |
| <1 μm | 33.84 | 29.64 | 28.30 |
| 1–2.5 μm | 3.74 | 3.33 | 2.99 |
| 2.5–4 μm | 10.80 | 11.86 | 10.80 |
| 4–10 μm | 41.48 | 45.40 | 45.66 |
| 10–15 μm | 10.14 | 9.77 | 12.25 |

distribution, which presented a maximum percentage of particles being at approximately 0.7 μm ; a shoulder was observed at approximately 1.8 μm . BD-B and C both displayed a bi-modal number-weighted size distribution with the highest proportion of particles being approximately 0.9 and 2.1 or 1.8 μm for BD-B and BD-C, respectively.

The mass distribution of BD-A demonstrated that the highest proportion of particles were approximately 2.5 μm which was slightly larger ($\sim 3 \mu\text{m}$) in samples BD-B and BD-C. The DustTrak determination of size fractions identified that the majority of BD particles (A, B, and C) were within the <1 and 4–10 μm mass-fractions.

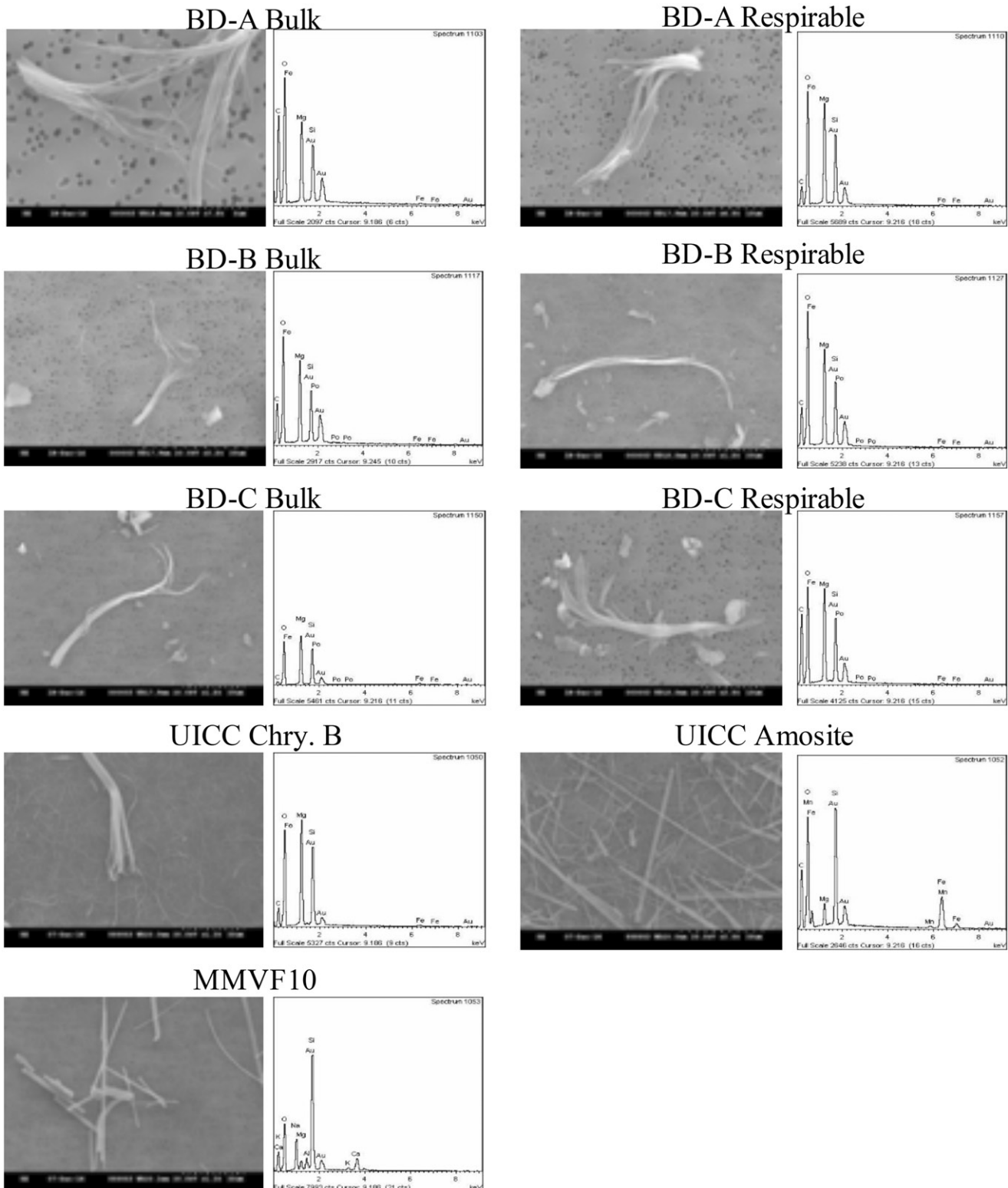


Figure 1. Representative SEM micrograph and EDX spectrum of pristine samples, including three bulk break debris (BD) samples, three respirable BD samples, UICC chrysotile B asbestos, amosite asbestos, and MMVF10.

Morphology (qualitative and quantitative) – SEM and TEM

As shown in **Figure 1**, the bulk version of all the BD was found to consist of mainly particles ranging in size range from single to tens of microns in diameter while particles containing embedded fibers, and ‘free’ fibers of a few microns up to hundreds of microns in length were also observed. Note that the use of the term ‘free’ here refers to fibers not held within the matrix, and can be single fibers or fibrillated fiber bundles. EDX analysis of particles which did not show obvious signs of protruding fibers at their surface, were identified as consisting of silicon, magnesium, and carbon, which may indicate the presence of chrysotile, but this was not confirmed. Iron and chromium were also present on the spectrum, however, as the second peak used to identify these elements was not clearly evident, these were not thought to be present.

Fibrillated bundles of WHO classified respirable and non-respirable fibers as well as particles with a chemical composition similar to chrysotile (two prominent peaks corresponding to Mg and Si), were observed and classified by EDX as chrysotile asbestos. Amosite displayed characteristically prominent Fe peaks which were absent from the BD samples and chrysotile (EDX does not have the sensitivity to identify the low concentrations of Fe typically found in chrysotile). This suggests that amosite or other iron containing amphiboles (e.g. tremolite (1.5–5% FeO) and actinolite (5–16% FeO); Van Orden 1964) were not present. This was further supported when considering morphology; the straight, rigid fiber appearance of the amphiboles was not observed within the BD. After isolation of a respirable fraction, the BD dusts retained their sample morphological diversity.

Quantitative analysis as summarized in **Table 2** shows that when comparing the bulk and isolated respirable fractions, the percentage of WHO-classified respirable fibers decreased in all three BD samples by on average 5.2% to account for ~15–17% of the respirable fraction. These respirable fibers possessed an average length of ~11 μm . The WHO classified ‘non-respirable’ fibers also showed a reduction in the isolated fraction to account for on average 12.3% across the three BD samples (11.1–13.8%) with an average length of 4 μm . As these ‘non-respirable fibers’ are clearly found within the respirable fraction, the classification is based on these entities not meeting the morphological characteristics of a fiber (i.e. length $>5 \mu\text{m}$, diameter $<3 \mu\text{m}$, and an aspect ratio of $>3:1$) rather than their inability to penetrate into the respirable zone. Indeed, the average diameter across the three BD samples was 0.6 μm making them clearly respirable, but with a length $< 5 \mu\text{m}$, they do not meet the minimum length threshold. In the assessment of fiber length distributions for all BD samples, the majority of fibers were found to $<10 \mu\text{m}$ (72.5% of BD-A, 74.9% of BD-B, and 85.3% of BD-C, respectively).

Crystallinity

The crystal structure, determined by XRD (**Figure S2**), identified that all of the ‘asbestos’-containing BD samples presented peaks characteristic of the UICC-Chry-B sample

which was run in comparison, including those at 7.26, 3.65, 2.45–2.55, and 2.1 \AA . A further crystal structure was identified in the XRD spectra for the BD samples, at approximately 3.05 \AA , which did not appear on the trace for chrysotile. Moreover, the combination of peaks that indicate the presence of amosite, as observed in the amosite reference material, was not reproduced in the XRD spectrum of the BD samples, therefore the BD was not believed to be associated with amosite.

Modeled lung deposition

The deposition efficiency in the human alveolar region was determined for the respirable fraction of the BD samples using the Multiple-Path Particle Dosimetry model version 3.04 (Applied Research Associates, Inc., Albuquerque, New Mexico, USA) (Anjilvel and Asgharian 1995; Price et al. 2002). The particle input parameters (MMAD and GSD) were derived from the APS analysis (**Table 1**) while the exposure conditions were modified to simulate light exercise (elevated breathing frequency and tidal volume) reflecting an active work situation (AGS 2014). The aerosol concentration was set at 4 mg/m^3 which is the maximal respirable workplace exposure limit (WEL) for low toxicity particulates (HSE 2005). This concentration was selected to take an inherently conservative approach (i.e. maximizing particle deposition) and does not assert that chrysotile containing dusts should be viewed as low toxicity dusts. Based on these input values (full details provided in **Table S4**), 10.00% of BD-A, 9.95% of BD-B, and 9.52% of BD-C would deposit within the alveolar region.

Characterization of material after ALF incubation

Particulate dissolution – gravimetric analysis & assessment of effluent fluid

The dissolution of asbestos-containing BD samples was shown to be consistent in all three samples, this was evident in both the gravimetric analysis of recovered sample (**Figure 2(A)**) and in the assessment of leached elements (**Figure 3(A,C,E)**).

As shown in **Figure 2(A)**, only 40% of each BD sample was recovered after 2 weeks with no further leaching observed after this time. The mass lost was statistically significant after the 14 and 42 days for BD-A and 7, 14, and 42 days incubation in ALF for BD-B and -C. The observed dissolution of BD corresponded well with the analysis of leached Fe and Mg (**Figure 3(C,E)**), as the detection of these analytes reached almost their maximum within 2 weeks. As shown in **Figure 3(A)**, the release of Si was slightly different as while there was rapid release during the first few days and weeks, a substantial amount was also released during 14 and 42 days. These observations also correlate well with the behavior of the UICC-Chry-B control material. In relation to mass, a rapid reduction occurred during the first 2 weeks with less than 50% recovered after this period (**Figure 2(B)**), which corresponded to leaching of Si (**Figure 3(B)**), Fe (**Figure 3(D)**), and Mg (**Figure 3(F)**) into the effluent fluid.

Table 2. Geometric analysis of chrysotile-containing BD samples before and after isolation of respirable fraction.

| | | | BD-A | | BD-B | | BD-C | |
|--|----------------------------------|------------------------------------|--------------------------|-------------------------|-------------------------|-------------------------|-------------------------|------------------------|
| | | | Bulk | Resp. | Bulk | Resp. | Bulk | Resp. |
| Particulates | Particles - no visible fibres | % | 40.04 | 39.08 | 24.64 | 30.73 | 33.66 | 30.90 |
| | | Average Diameter (μm) | 2.67 (± 1.63) | 2.89 (± 1.89) | 2.72 (± 1.90) | 2.27 (± 1.38) | 1.75 (± 0.81) | 1.97 (± 1.12) |
| | Particles - embedded fibres | % | 20.12 | 31.78 | 35.65 | 43.31 | 28.48 | 39.95 |
| | | Average Diameter (μm) | 10.63 (± 11.26) | 5.47 (± 3.97) | 8.00 (± 7.14) | 5.56 (± 3.80) | 6.45 (± 7.58) | 4.10 (± 2.46) |
| 'Free' Respirable fibres ⁽¹⁾ | % Fibres | | 25.05 | 17.08 | 19.14 | 14.90 | 22.56 | 15.16 |
| | Average Length (μm) | | 13.13 (± 10.92) | 11.84 (± 8.52) | 11.54 (± 7.78) | 11.78 (± 9.27) | 11.61 (± 9.24) | 9.50 (± 5.67) |
| | Average Width (μm) | | 0.84 (± 0.71) | 0.74 (± 0.63) | 1.07 (± 1.19) | 0.93 (± 0.76) | 0.69 (± 0.69) | 0.78 (± 0.90) |
| 'Free' Non-WHO defined fibres ⁽²⁾ | % Fibres | | 14.78 | 12.06 | 20.57 | 11.06 | 15.29 | 13.99 |
| | Average Length (μm) | | 5.57 (± 7.18) | 4.00 (± 3.03) | 6.42 (± 16.96) | 4.58 (± 5.20) | 3.65 (± 3.35) | 3.63 (± 2.68) |
| | Average Width (μm) | | 0.85 (± 1.43) | 0.55 (± 0.89) | 0.56 (± 1.19) | 0.83 (± 1.38) | 0.36 (± 0.61) | 0.36 (± 0.52) |
| Length Distribution (% Fibres) | <5 | | 33.51 | 38.37 | 50.00 | 40.81 | 40.07 | 47.41 |
| | 5 - 10 | | 32.99 | 34.14 | 27.71 | 34.08 | 34.53 | 37.93 |
| | 10 - 15 | | 17.53 | 14.80 | 11.45 | 12.11 | 12.70 | 8.05 |
| | 15 - 20 | | 4.12 | 7.25 | 4.22 | 7.17 | 6.19 | 2.87 |
| | 20 - 30 | | 7.73 | 3.02 | 1.81 | 3.59 | 3.26 | 2.87 |
| | 30 - 40 | | 2.58 | 0.91 | 2.41 | 0.90 | 1.95 | 0.57 |
| | 40 - 50 | | 0.00 | 0.91 | 0.60 | 0.45 | 0.65 | 0.29 |
| | 50+ | | 1.55 | 0.60 | 1.81 | 0.90 | 0.65 | 0.00 |

The distinction between a 'free' respirable fiber and a 'free' Non-WHO-defined fibers is based on the WHO fiber counting convention which directs a respirable fiber as possessing a length $>5 \mu\text{m}$, diameter $<3 \mu\text{m}$, and an aspect ratio of $>3:1$.

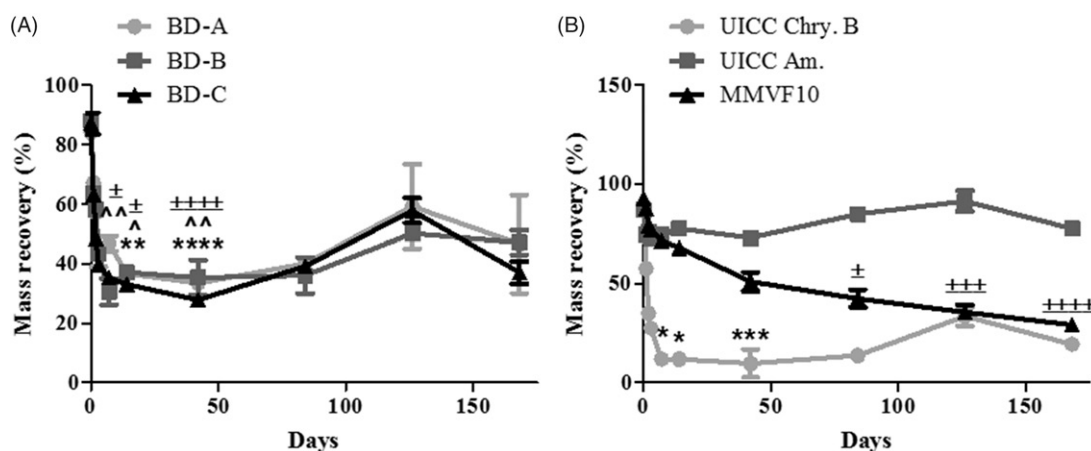


Figure 2. Mass recovery, in percent, of (A) asbestos-containing break debris (BD-A, BDB, and BD-C), and (B) chrysotile, amosite and MMVF10, after incubation in ALF for 0–168 days. The data are expressed as mean \pm SD of four replicates. Statistical significance is shown for $p < 0.05$ (*), $p < 0.01$ (**), $p < 0.005$ (***), and $p < 0.001$ (****) for BD-A/chrysotile, $p < 0.05$ (\wedge) and $p < 0.01$ ($\wedge\wedge$) for BD-B, or $p < 0.05$ with (\pm), $p < 0.005$ ($\pm\pm\pm$), and $p < 0.001$ ($\pm\pm\pm\pm$) for BD-C/MMVF10.

The total release of Si and Mg was greater from UICC-Chry-B compared to asbestos-containing BD owing to the pure (i.e. high Mg and Si) nature of the UICC-Chry-B, and

the level of other (matrix) contaminants present in the BD samples. It should be noted that this assessment relates to absolute values of leached materials, proportionally the

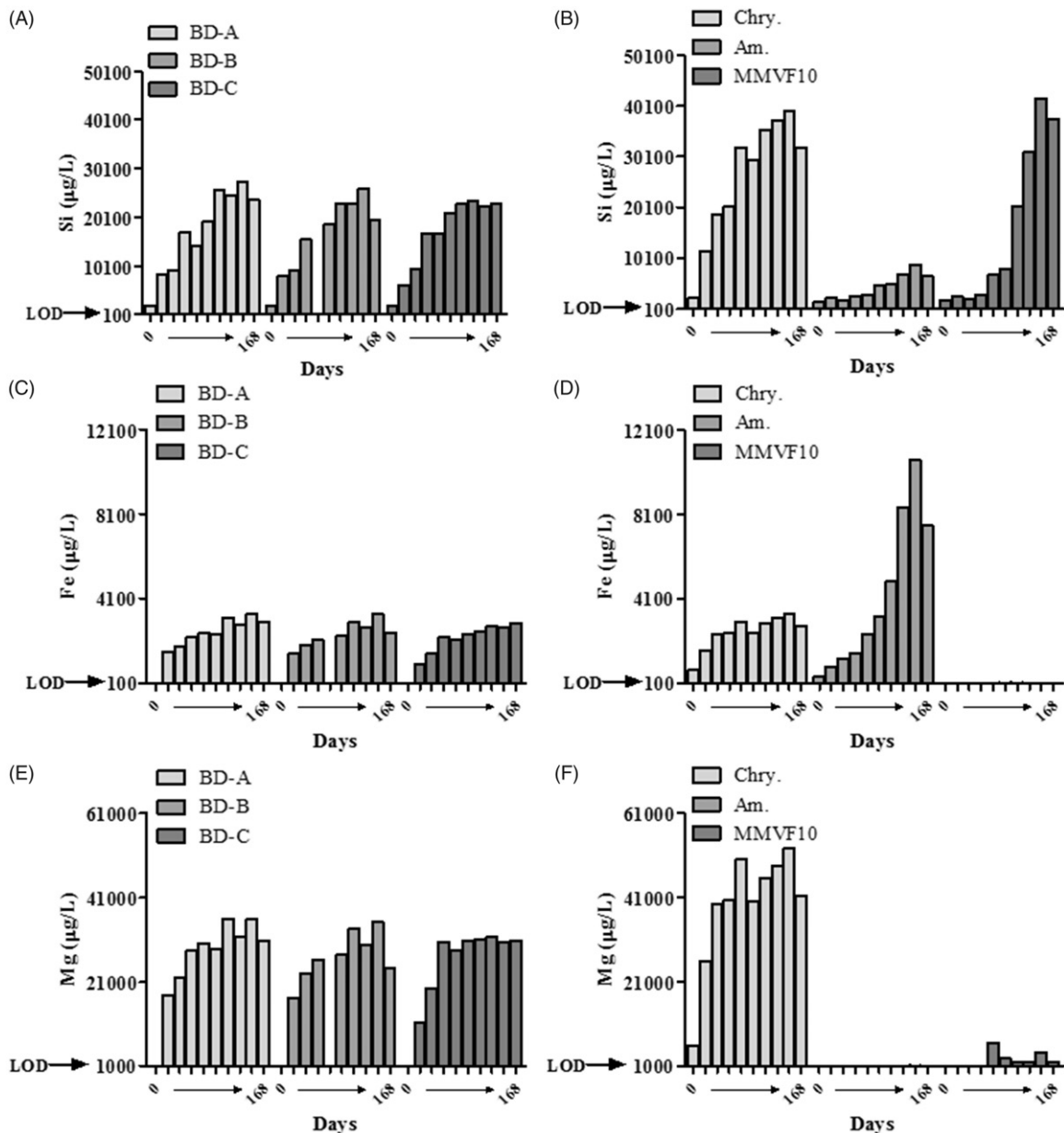


Figure 3. Quantification of Si (A and B), Fe (C and D), and Mg (E and F) in effluent fluid released from asbestos-containing BD (A, C, and E) and chrysotile, amosite, and MMVF10 (B, D, and F) after incubation in ALD for 0–168 days. The data are expressed as μg solute per liter of fluid.

release of Si and Mg may have been less variable when comparing the asbestos-containing BD and UICC-Chry-B, however, this was not assessed.

The dissolution of the more biodurable amphibole sample was as expected, with amosite recovery being particularly high, with no more than 20% lost throughout the incubation time (Figure 2(B)) and the main leachate being Fe (Figure 3(D)). The dissolution of more biosoluble MMVF10 was shown to be linear with incubation time, with 30% remaining at the end of the 168-day incubation period (Figure 2(B)) and incremental leaching of Si throughout the time course (Figure 3(B)). The mass-loss of MMVF10 was found to be statistically significant after 84, 126, and 168 days incubation in ALF.

When considering the dissolution rates shown in Table 3, it was evident that over time the dissolution rates of all materials decreased, according to mass loss, while in terms

of Si release, both amosite and MMVF10 were shown to present a relatively stable rate of dissolution. However, in general, the dissolution rates of either total sample mass or leached Si confirm what was observed in the previous analysis. The rates of dissolution for the BD samples and for chrysotile are all relatively high during the first 2 weeks of exposure and dramatically decrease after this time.

Surface charge – zeta potential

Prior to incubation and at each timepoint the surface charge of all test materials was measured at a biologically relevant pH value of 5 (Figure S4). This value addresses the reduced pH range of intracellular lysosomal pH (Luoto et al. 1998) as well as extracellular hydrolytic compartment of a macrophage (Haka et al. 2009). At pH 5, all the pristine BD samples presented a negative surface charge with a trend

Table 3. Dissolution rates of three asbestos-containing BD and references samples incubated in ALF from 0 to 168 days.

| Dissolution rate | Time point | BD-A | BD-B | BD-C | UICC-Chry-B | UICC amosite | MMVF10 |
|--|--|--------------------|--------------------|--------------------|--------------------|------------------|-------------------|
| Determined from gravimetric analysis of mass loss. ($\mu\text{g/h}$) | T1 | 153.02 \pm 13.90 | 168.85 \pm 20.96 | 129.79 \pm 26.51 | 179.37 \pm 25.73 | 75.31 \pm 5.60 | 145.21 \pm 8.72 |
| | T2 | 107.24 \pm 7.76 | 129.32 \pm 27.04 | 89.84 \pm 19.33 | 143.49 \pm 50.44 | 32.14 \pm 3.37 | 77.24 \pm 8.39 |
| | T3 | 88.54 \pm 10.03 | 93.47 \pm 17.50 | 90.69 \pm 8.42 | 92.29 \pm 25.79 | 24.83 \pm 0.57 | 53.12 \pm 4.70 |
| | T7 | 40.12 \pm 7.45 | 12.74 \pm 2.27 | 43.1 \pm 12.60 | 61.35 \pm 19.82 | 11.65 \pm 1.32 | 38.00 \pm 10.88 |
| | T14 | 22.95 \pm 3.32 | 26.52 \pm 5.08 | 18.42 \pm 4.08 | 20.34 \pm 5.13 | 5.31 \pm 0.74 | 19.56 \pm 2.60 |
| | T42 | 8.48 \pm 0.96 | 10.74 \pm 2.10 | 6.53 \pm 2.31 | 11.3 \pm 4.01 | 1.9 \pm 0.18 | 8.8 \pm 0.98 |
| | T84 | 3.54 \pm 0.52 | 3.57 \pm 1.31 | 2.86 \pm 0.66 | 4.4 \pm 2.52 | 0.6 \pm 0.07 | 5.44 \pm 1.04 |
| | T126 | 1.5 \pm 0.86 | 2.61 \pm 0.21 | 1.26 \pm 0.20 | 1.98 \pm 0.33 | 0.25 \pm 0.21 | 3.49 \pm 0.89 |
| | T168 | 1.82 \pm 1.51 | 1.29 \pm 0.32 | 2.13 \pm 0.49 | 1.76 \pm 0.42 | 0.46 \pm 0.10 | 2.99 \pm 0.33 |
| | Determined from ICP analysis of leached Si ($\mu\text{g/h}$) | T1 | 11.64 | 11.07 | 6.38 | 14.43 | 2.29 |
| T2 | | 6.88 | 8.44 | 4.96 | 12.86 | 0.81 | 2.31 |
| T3 | | 7.92 | 7.70 | 7.52 | 7.83 | 0.72 | 2.05 |
| T7 | | 3.21 | – | 2.93 | 6.66 | 0.34 | 2.70 |
| T14 | | 2.08 | 2.36 | 1.73 | 2.02 | 0.34 | 1.49 |
| T42 | | 0.98 | 1.14 | 0.63 | 1.37 | 0.11 | 1.11 |
| T84 | | 0.43 | 0.40 | 0.33 | 0.60 | 0.08 | 0.90 |
| T126 | | 0.29 | 0.41 | 0.20 | 0.35 | 0.07 | 0.68 |
| T168 | | 0.21 | 0.14 | 0.23 | 0.21 | 0.04 | 0.48 |

The dissolution rate is expressed based on the total mass loss as well as leached Si. The data represent the mean of four independent replicates. For gravimetric mass loss the standard deviation (SD) is provided; analysis by ICP involved pooling of replicates prior to analysis, therefore SD is not available.

towards an increasingly negative charge with incubation in ALF. UICC chrysotile B showed a similar pattern of a strong positive charge which, with the exception of Day 14 incubation in ALF was negatively charged from Day 3. No measurements were taken at Days 126 and 168 as recovery of the remaining sample was insufficient due to dissolution. Both amosite asbestos and MMVF10 displayed a negative charge with the later fiber showing a progressive trend towards a less negative surface charge. A similar pattern was noted at other pH values of 3, 7, and 9 (Figure S5(A–C)) with the pristine BD samples showing a positive surface charge at pH 3.0 which rapidly transitioned to negative with 24 hrs in ALF.

Reactive oxygen species – EPR

The formation of free radicals, namely superoxide anions, by all test materials was assessed by EPR using the Tempone-H spin trap (Figure S6). The positive control, pyrogallol, produced significant ($p < 0.05$) levels of ROS. None of the test materials produced a significant increase in superoxide compared to the vehicle control. Each particle was tested for interference, by performing the test in the absence of Tempone-H, and none was observed.

Morphology (qualitative and quantitative) – SEM and TEM

After incubation of BD in ALF for 0 days, each sample was observed to be similar to the examination of pristine respirable material. During the course of the incubation in ALF (0–168 days), the average length of free respirable fibers in BD-A was relatively consistent and ranged between 7 and 12 μm , with diameters varying between 0.5 and 1.4 μm ; neither of these parameters were observed to reduce or increase in any obvious pattern during incubation. However, the proportion of fibers did change; the percentage of free respirable fibers present in BD-A reduced from 22% at Day 0 to 4% at Day 126 with no free respirable fibers observed after 168 days incubation in ALF. Similarly, a reduction in non-WHO fibers from 10% at Day 0 to 2% at Day 126 was

noted (see Table S1 for full analysis). These same trends in morphological change were observed for both BD-B and BD-C, details of which can be seen in Tables S2 and S3 as well as representative SEM images in Figures S7–S9. The length distribution of fibers within each BD sample was also not found to be different from those determined in the pristine samples with the largest proportion of fiber lengths observed with the <5 and 5–10 μm categories. This was a consistent observation for the duration of the test (0–168 days of incubation in ALF), however, it was evident from the counts that the actual number of fibers in each category reduced with a linear relation to incubation time, and few were left. UICC-Chry-B was also shown to be relatively unchanged from observations made of the pristine material and those made at Day 0 of incubation in ALF. After 7 days incubation in ALF, however, the appearance of chrysotile was dramatically different, as was that of the BD samples (Table S5; Figures S7–S9). The majority of chrysotile fibers in the pristine sample were found within the <5 and 5–10 μm length categories (84.9%); which was a trend observed throughout most of the study. However, as was shown for BD samples, the frequency of chrysotile fibers dramatically decreased in relation to incubation time, and after 2 weeks very few chrysotile fibers were observed. Alongside this, the EDX spectrum identified a general loss of Mg from these samples which was also evident in the EDX spectrum of all BD samples. This loss corresponded to an observable decrease in the amount of fibers present, either embedded in resin or free. After 84 days of incubation in ALF (Figure S9), these effects were further exaggerated, and in all cases, BD and chrysotile, there was very little evidence of either free respirable fibers or non-WHO fibers being present. This overall reduction appears to be relatively rapid, with decline in fibers present and a rise in proportionate particles present within the first 14 days of incubation in ALF. Similar analysis by TEM (Figure 4) corroborated these effects; the presence of fibrous material in all three BD samples were clearly observed in the pristine samples, while at the end of the 168-day incubation period in ALF, the presence of fibers was either very low or non-existent. The

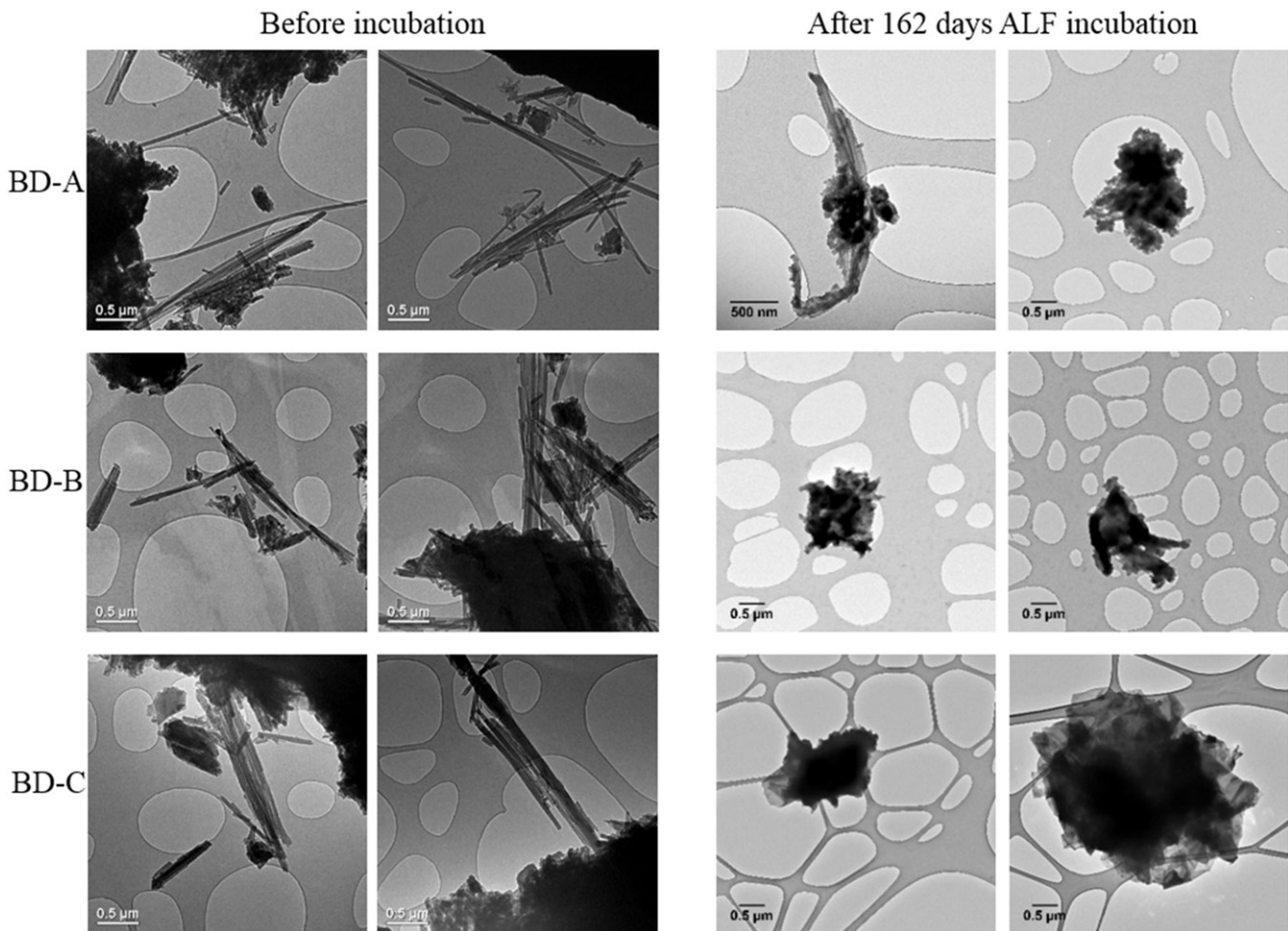


Figure 4. TEM micrographs of asbestos-containing BD prior to incubation in ALF and after 168 days incubation in ALF.

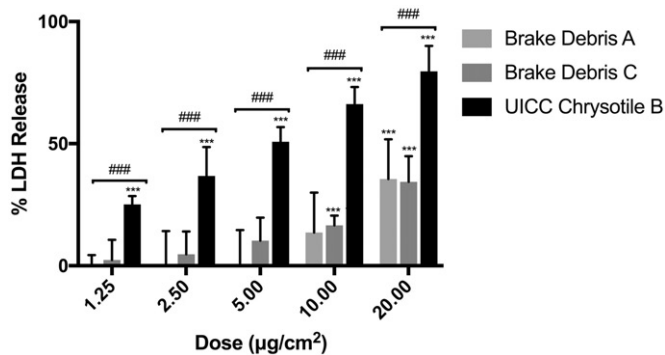


Figure 5. Cytotoxicity analysis of respirable brake debris particles in relation to UICC chrysotile B asbestos fibers. Data are expressed as mean \pm SD of four independent replicates. *** $p < 0.001$ vs. vehicle control, ### $p < 0.001$ vs. UICC chrysotile B.

corresponding geometric analysis of what is represented in Figure 4 can be seen in Figure S10. The chrysotile containing BD samples incubated in ALF for 168 days were examined for presence of particles, free fibers, and fibers embedded within particles; both BD-B and BD-C were found to consist of what appeared to 100% matrix material, BD-A was shown to consist of approximately 75% matrix material, with the remainder being fibers embedded within matrix. No free fibers were observed.

Macrophage interactions

Assessment of the cytotoxic effects of BD in relation to UICC-Chry-B asbestos fibers showed a dose-response increase in LDH release from differentiated THP-1 cells. As shown in Figure 5, co-incubation with even low levels of UICC-Chry-B caused upwards of 20% LDH release while the same mass of either BD-A or BD-C led to no appreciable release. Significant release occurred at doses above 10 $\mu\text{g}/\text{cm}^2$ yet at all doses tested, this was significantly lower than pure chrysotile ($p < 0.001$). As such, a non-cytotoxic dose of 2.5 $\mu\text{g}/\text{cm}^2$ was selected for further experiments.

Using a combination of SEM and TEM analysis, the interaction of differentiated THP-1 macrophages with BD-A, BD-C, and UICC-Chry-B was assessed. As summarized in Figure 6, macrophages treated with BD showed a range of morphologies, with occasional surface bound matrix particles as evident in Figure 6(a). As shown in Figure 6(b) and at higher magnification in Figure 6(c), the debris could consist of both angular resin fragments and also, short chrysotile fragments. However, where long fibers were present, these protruded from the macrophage in a morphology akin to frustrated phagocytosis (Figure 6(a), white chevron). TEM analysis showed the internalization of such particulates and matrix agglomerates containing chrysotile fragments were often noted either internalized (Figure 6(d)) or in the

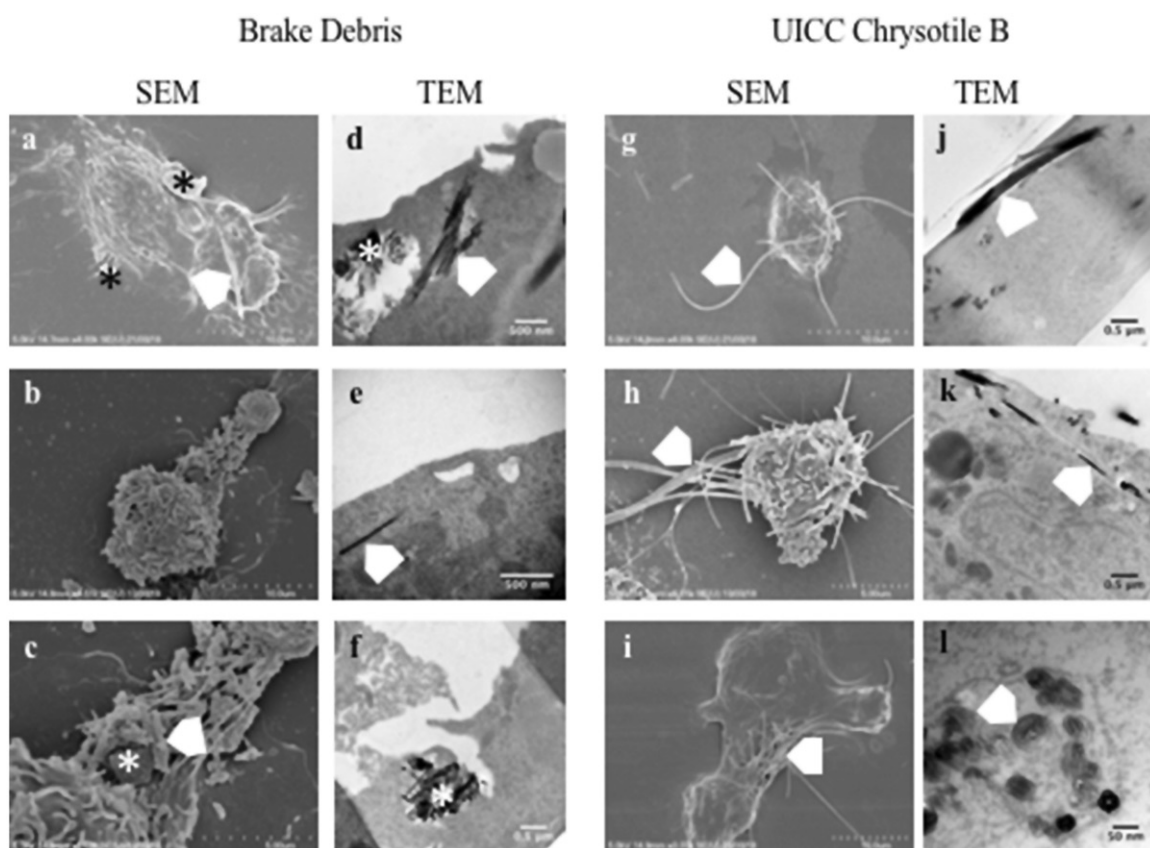


Figure 6. Electron micrographs of differentiated THP-1 macrophages incubated with brake debris (a–f) or UICC chrysotile B asbestos (g–l). The asterisk (*) indicates particulate brake debris while the white chevron indicates chrysotile fibers or fragments.

Table 4. Particle/fiber uptake by THP-1 macrophage-type cells ($N = 3$).

| Particulates | Total cells | No particulates (%) | | Complete uptake (%) | | Incomplete uptake (%) | |
|--------------|-------------|---------------------|--------|---------------------|--------|-----------------------|--------|
| | | Mean | St dev | Mean | St dev | Mean | St dev |
| Vehicle | 1847 | 100.0 | 0.0 | 0.0 | 0.0 | 0.0 | 0.0 |
| BD-A | 1866 | 47.5 | 6.9 | 50.6 | 6.8 | 1.8 | 0.2 |
| BD-C | 1821 | 37.6 | 5.5 | 61.6 | 5.3 | 0.8 | 0.3 |
| UICC-Chry-B | 1858 | 57.0 | 3.9 | 4.9 | 2.3 | 38.1 | 5.3 |

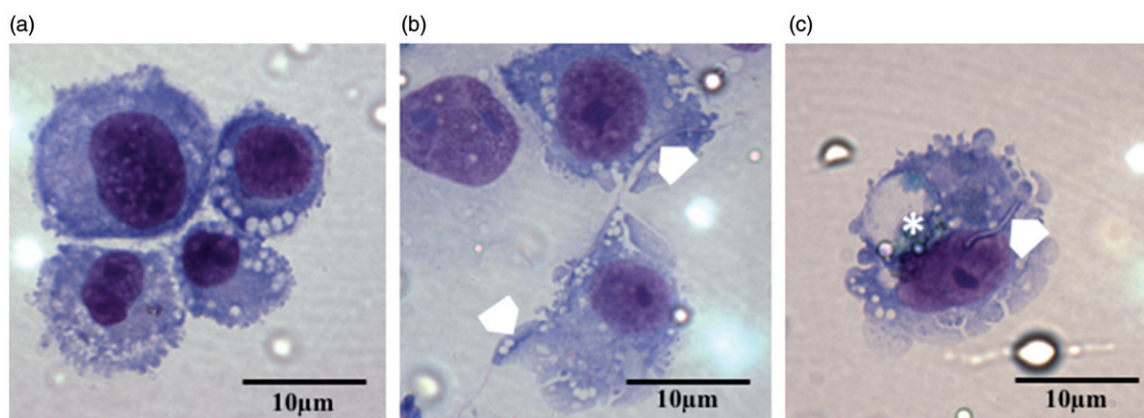


Figure 7. Representative images of differentiated THP-1 macrophages treated with and (a) vehicle control, (b) $2.5 \mu\text{g}/\text{cm}^2$ of UICC chrysotile B, or (c) Brake debris. Image (a) shows the normal cellular appearance of an activated macrophage with no particulates. The white chevrons on image (b) show the presence of a long chrysotile fiber which penetrates two macrophages. Image C shows the presence of a short chrysotile fragment (white chevron) fully internalized by a macrophage as well as the presence of resin matrix held within a large vacuole (*). All images at $\times 100$ magnification.

process of phagocytosis (Figure 6(f)). What appear to be free chrysotile were also noted internalized yet as shown in Figure 6(d,e), these were often too short to be classified as a fiber. In contrast, co-incubation with chrysotile fibers led to many macrophages displaying prominent protrusions of chrysotile where attempted internalization has failed (Figure 6(g-i)). TEM analysis also showed longer fibers penetrating into the cell (j) and where these were observed in a transverse position, the coiled silicate layer of the chrysotile was clearly visible (l). Both in terms of chrysotile and BD, the internalized or partially internalized particulates often appeared to be surrounded by a membrane.

As summarized in Table 4 and Figure 7, optical analysis of cells showing either no internalized particulates, fully internalized particulates (complete uptake) or only partially internalized particulates (incomplete uptake) showed marked differences between the BD and chrysotile samples. As would be expected, the vehicle control-treated cells showed no evidence of particulates what so ever while the UICC-Chry-B-treated cells showed just over half (57%) of the cells with no particles or fibers. However, 38.1% showed evidence of fibers protruding from the cell membrane showing incomplete uptake which may hinder of cell mobility and as such, lung clearance. A clear example of this can be seen in Figure 7(b) where a long chrysotile fiber can be seen passing through two macrophages, neither of which can encompass the whole fiber.

Only a small proportion of cells showed evidence of complete uptake of fragments of chrysotile. In contrast, for both BD-A and BD-C samples, the majority of cells showed evidence of complete uptake (50.6 and 61.6%, respectively) and to the most part, these were fragments of resin. As shown in Figure 7(c), short chrysotile fibers were noted yet often, fragments of resin (~1–2 μm in diameter) were often noted. A very small proportion of the BD-treated cells showed fibers protruding from the surface (0.8–1.8%) which likely reflects the relatively low proportion of long free fibers in the BD when compared with native chrysotile.

Discussion

There is well-documented historical exposure of mechanics to chrysotile following machining and replacement of chrysotile containing brake pads. Despite this exposure to a known carcinogen at varying levels (including those above prescribed limits), case study accounts of mesothelioma in mechanics have not translated into evidence of excess risk as determined by numerous epidemiological studies and meta-analysis (Poland and Duffin 2019). It is important to recognize that such conclusions are not universally shared yet the purpose of this study was to determine if there is a possible physicochemical basis for altered pathogenicity.

In the case of particle and fiber toxicology, two main driving forces behind toxicity are the physicochemical characteristics of the particulate(s) and dose. Obviously, there are other influencing factors such as health status, age, genetic susceptibility yet the dose, morphology, and physicochemical properties are of primary importance. Chrysotile

fibers within brake pads are bound within a phenolic resin, subjected to heat and pressure during the production process and high shear stresses during the grinding of the surface and braking. Given these factors, it is entirely plausible that the morphological and physicochemical properties of chrysotile may be altered in comparison to the virgin chrysotile 'asbestos' fibers. Indeed, Weir and Meraz (2001) analyzed the particulates liberated from brake pads containing $50 \pm 10\%$ chrysotile. They found that the released material was mostly resin matrix yet some fibrous material, compositionally and morphologically consistent with chrysotile were also found, although the majority of which were bound to a resin matrix. Such findings have been noted in other studies (Lynch 1968; Hatch 1970; Rohl et al. 1976) and certainly indicates the possibility of modification such as bound resin particles which would alter the aerodynamic properties of the fiber.

In relation to key morphological and physicochemical properties that can influence the toxicity of particulate and of relevance to the brake pad chrysotile are:

- Fiber length/diameter
- Coating/matrix interactions
- Biodurability
- Surface reactivity

Furthermore, and considering chrysotile and the production/liberation conditions specifically, the potential for heat modification as well as presence of amphiboles as a contaminant in relation to the 'amphibole hypothesis' should also be considered. The characterization of the BD determined above is considered in relation to these factors in particulate pathogenicity.

Fiber length

The fiber pathogenicity paradigm (FPP) has a robust structure/toxicity relationship that enables the prediction of the pathogenicity of fibers depending on their length, thickness, and biopersistence (Donaldson et al. 2010; Braakhuis et al. 2014). The impact of fiber length on toxicity has been known for many decades (Stanton et al. 1977; Davis et al. 1986) with fibers $>5 \mu\text{m}$ seen as the key length regarding fiber-type toxicity and regulation (Poland et al. 2018). Within the respirable fractions of the three BD samples, 15–17% of particulates measured met the WHO criteria and had an average length of around 11 μm . In addition, all three samples showed a small yet toxicologically important sub-fraction of 'free' fibers which meet the WHO classification of a respirable fiber. In relation to the FPP, this sub-fraction of long fibers represents a plausible biologically effective dose and as such, a fiber-type hazard which would normally be a cause for concern. However, as discussed later, biodurability is also a key component of the FPP as it effects the persistence of long fibers in the lung and marks a key distinction in the relative toxicity between high toxicity fibers such as amosite and low toxicity fibers such as MMVF10 glass fiber.

Biodurability

The biopersistence of a particle or fiber is considered as a combination of chemical dissolution in the biological milieu (i.e. biodurability) and physical clearance such as by alveolar macrophages in the lung. The comparisons within this study have been relatively broad as we have compared chrysotile with MMVF10 (a biosoluble glass fiber) and amosite, a bio-durable amphibole. *In vivo* studies have shown biopersistence half-life ($WT_{1/2}$) for these benchmark fibers of 14.5 days for MMVF10 (Hesterberg et al. 1993) and 418 days for amosite (McConnell et al. 1994). However, even within materials classified as ‘chrysotile,’ there can be considerable variation in biopersistence. At the least biopersistent end of the spectrum is Calidria chrysotile which has been shown to have a $WT_{1/2}$ of only 7 h after inhalation (Bernstein et al. 2005). This differs substantially from $WT_{1/2}$ for ‘Brazilian’ and ‘Canadian’ chrysotile’s of 1.3 and 11.4 days, respectively (Bernstein et al. 2004; 2005). Even longer biopersistence half-lives have been reported with different samples of Canadian origin chrysotile ranging from 47.6 to 116 days (Coin et al. 1992; Searl 1997).

The basis for such variability can be different experimental design and analysis as standardized approaches such as that of Note Q within European regulation (Regulation (EC) No 1272/2008 of the European Parliament and of the Council of 16 December 2008 on classification, labelling and packaging of substances and mixtures, amending and repealing Directives 67/548/EEC and 1999/45/EC, and amending Regulation (EC) No 1907/2006. Available at: <https://eur-lex.europa.eu/legal-content/EN/ALL/?uri=CELEX:32008R1272>) for mineral fiber biopersistence (Bernstein and Riego Sintes 1999). However, variation can also stem from physicochemical differences in chrysotile samples as biopersistence is a function of fiber size and composition. Such differences account for the rapid clearance of Calidria chrysotile as the long fibers are actually formed of multiple short fibrils which once dispersed can be cleared rapidly. Differences in fiber composition (e.g. relative proportion of biosoluble components such as Mg in the brucitic layer) as well as degree of fibrillation effecting both surface area and accessibility of biosoluble components may all effect dissolution and clearance (Poland and Duffin 2019).

Regarding the test materials, the results have shown that when incubated in a low pH ALF, all three BD samples, as well as the UICC-Chry-B, demonstrate a rapid and progressive trend of reduction in mass and fiber frequency. This concordance in mass loss between BD and chrysotile is likely due to the chrysotile component (up to 50% of the total mass composition; Weir and Meraz 2001). As recently reviewed (Poland and Duffin 2019), the dissolution and clearance of chrysotile from the lung can be viewed as a two-step as described by Gualtieri (Gualtieri 2018). Firstly there is a rapid dissolution of magnesium from the chrysotile which is known to be susceptible to leaching especially in acidic conditions (Virta 2002) as found in the phagolysosome of a macrophage. The second step is the gradual breakage of the weakened fibrous metastable silicate pseudomorph although this may be at a slower rate than the

dissolution of the brucitic layer (Gualtieri et al. 2018). In terms of the long fibers being the critical biologically effective dose within the mixed BD exposure, it is this dissolution and fragmentation of the sub-fraction of long chrysotile fibers that may be critical to the formation of chronic disease states such as MM. In relation to this, the data demonstrate a reduction in the frequency of long fibers and as such may represent a progressive reduction in biologically effective fiber dose over time.

The rapid dissolution of ‘chrysotile’ (either as a component of BD or as the comparator control) and MMVF10 in comparison to the more durable amosite correlates well with published *in vitro* dissolution rates. At pH 7, amosite asbestos was shown to have an *in vitro* dissolution rate (K_{dis}) of <1 while the more soluble MMVF10 had a rate of 300 (Hesterberg et al. 2012). More recently, (Gualtieri et al. 2018) undertook a comparative *in vitro* study of UICC chrysotile B and UICC amosite asbestos using a static approach similar to that used herein, at pH 4. The calculated dissolution time for chrysotile was in the range of 94 (± 26) days which is a fraction of the time calculated for UICC amosite of 74 (± 7) years. Considering the behavior of these benchmark fibers in relation to the observed rates of dissolution in the BD samples shown in Table 3, it would be expected that fibrous components of BD would be cleared at rates more akin to chrysotile. Indeed, this has been shown to be the case whereby the $WT_{1/2}$ of long fibers in chrysotile containing break debris was shown to be ~ 30 days in rats while a biopersistent amphibole (crocidolite) had a $WT_{1/2}$ was >1000 days (Bernstein et al. 2014).

Fiber/matrix interactions

The grinding of the brake pads produces a mixture of resin particulates, particles containing embedded fibers as well free fibers (fibrils and bundles). Where released material consists of chrysotile fibers fully embedded and enclosed within resin, it would possess the aerodynamic diameter (D_{ae}) and surface properties of the resin particle. As biological interactions occur at the surface of a particle, the toxicological impact of the chrysotile containing fragment would likely reflect that of resin alone. The exception would be if the resin component was bio-soluble as the encapsulating layer may degrade within the lung and release the embedded chrysotile. However, the chrysotile containing resin particle would need to be of sufficient size to encapsulate long chrysotile fibers or else would only contain short, easily cleared chrysotile fragments. Large resin particles owing to their greater D_{ae} would deposit with much lesser efficiency in the alveolar region than smaller particles.

Chrysotile fibers protruding from a resin matrix particle present an interesting particulate from a toxicological perspective. Long free fibers, owing the peculiarities of fiber D_{ae} can penetrate the alveolar region. However, those with a matrix attachment are likely to deposit with lesser efficiency as the additional density, drag properties and weight distribution across the fiber/matrix hybrid would likely serve to increase the D_{ae} , not reduce it. Despite this, characterization

of the respirable fraction of the BD has shown a large proportion of resin particles with protruding fibers (~40%). From a macrophage perspective, depending on size and length of protrusions, such particles may either be cleared with relative ease (smaller particles with short fiber protrusions) or present a considerable challenge both in terms of shape (longer fiber protrusion) and volume (larger particle).

In terms of free-fibers meeting the WHO criteria of a respirable fiber, these would be expected to behave and present the same toxicological hazard as any other chrysotile fiber of the same shape and size. However, this may not be the case if the process of being encased in resin forms a surface coating. Such a coating may modify the surface properties such as charge and reactivity which may serve to pacify the surface with implications for cellular interactions as has previously been noted for reactive quartz particles (Duffin et al. 2001). However, such a coating may also serve to form an insoluble barrier thereby reducing the rate of dissolution and increasing biopersistence; effectively forming a 'Catch-22' situation. Attempts to detect such a surface layer on free and protruding fibers using high-resolution TEM (Titan Themis 200, Thermo Fisher Scientific, Hillsboro, Oregon, USA) proved unsuccessful despite the high resolution owing to the limited electron density of the resin (data not shown).

Surface reactivity

Among the physicochemical properties affecting toxicity, those relating to the surface are of particular interest as it is the surface of particles and fibers which interact first hand with the surrounding target tissue and cells following deposition in the organism (Fubini 1997; Oberdorster and Graham 2018). As most recently discussed by Gualtieri (2018) in relation to a predictive model of mineral fiber pathogenicity, surface reactivity can play a role in particle/fiber toxicity. Indeed, attributes such as surface charge have been shown to influence respiratory toxicity of particles such metal oxides (Cho et al. 2012) and even polystyrene nanoparticles (Kim et al. 2016). In relation to chrysotile, the impact of surface charge on cell injury has been known for some time (Light and Wei 1977) whereby the highly charged surface of chrysotile can cause adverse membrane interactions (as demonstrated by high hemolytic activity). The characterization of UICC-Chry-B across a range of pH values confirm a high zeta-potential of up to +35mV. In comparison, at biologically relevant pH values, all BD samples rapidly present a negative charge. As such, considering charge mediated toxicity though binding of negatively charged cell membranes, the BD samples would be nonreactive. However, when considering a mixed sample such as the BD, it is unclear if the zeta potential value measured represents a homogenous (i.e. all particles/fibers possess the same measured charge) or an aggregate charge of the differing charges of differing particles and fibers. While this may seem like semantics, cellular interactions are with individual particles and not the entire received organ dose. Therefore, the presence of highly charged particulates within a mixed

sample may represent a biologically effective dose to those cells which encounter them. In relation to the BD, it is plausible that that the resin matrix components have a neutral/negative surface charge while free chrysotile fibers and fragments may possess a similar positive charge to that of the parent material. Fibers which are embedded or perhaps coated in resin would most likely have a decreased surface charge akin to the coating substance (likely dependent on the thickness of the coating).

The loss of surface charge with increasing incubation time in ALF is due to the loss of magnesium which is the source of the chrysotile fibers highly positive charge (Virta 2002). As such, even if the chrysotile within the BD maintained the same positive charge as the UICC-Chry-B, the results would suggest that within a low pH biological environment, the surface charge would progressively reduce to neutral owing to the loss of magnesium. As such, from a surface reactivity perspective impact of surface charge on cellular function would be limited to the shorter term.

The production of reactive oxygen species, leading in turn to oxidative stress and damage is seen as a key mediator of particle and fiber toxicity (Li et al. 2008). Within this study we also sought if incubation in simulated biological fluids could cause modifications in free radical generation. Such an evolution over time has been reported previously in relation to amphiboles (Andreozzi et al. 2017). Analysis of intrinsic ROS production by EPR showed no significant increase over vehicle control for any of the test samples indicating, that for the spin-trap Tempone-H at least, reactivity is minimal. However, while there is little evidence for intrinsic ROS production from the BD, interactions between cells such as macrophages and neutrophils may lead to enhanced production of ROS from the cells themselves (e.g. via respiratory bursts). Furthermore, the presence of oxidants such as hydrogen peroxide as a by-product of superoxide dismutation may interact with iron within the fibers themselves or within the brake matrix via Fenton reaction (Fe^{2+} oxidation) and the Haber-Weiss cycle (Fe^{3+} reduction) (Vallyathan et al. 1992) to generate hydroxyl radicals. The source of reactivity within the BD samples is, of course, not solely limited to the chrysotile component. Brake pads are composed of numerous materials that make up the combination of fillers, frictional additives, and abrasives, including iron particles which lead to higher reactivity in the biological milieu.

Overall, the relative reactivity of the BD when compared to pure chrysotile and amosite asbestos is reduced and as an aggregate material, would be expected to present much less of a hazard. However, the mixed nature of the BD samples means that a sub-fraction of the received BD dose (i.e. free, uncoated chrysotile fibers) may be reactive in the shorter term while undergoing dissolution.

Fiber heat modification

Due to the generation of friction, there is the possibility of heat modification of chrysotile during the grinding of the brake pads. While chrysotile asbestos has been widely used

due to its noncombustible and insulating capacity (e.g. in fire-proof suits), it is not actually impervious to change under heat. As described by Zaremba et al. (2010), heating of chrysotile leads to thermal decomposition due to the dehydroxylation of the chrysotile fibrils. With sufficient heat, this can result in the complete breakdown of the mineral structure and the formation of forsterite. The importance of this lies in the fact that forsterite has a very different structure, lower biodurability, and toxicity profile when compared to chrysotile (Gualtieri et al. 2012). Indeed, heat treatment has been suggested as a recycling strategy for chrysotile-containing materials (Gualtieri and Tartaglia 2000). The question of if heat generation during grinding could significantly modify chrysotile including the transformation to forsterite hinges on the heat generated. Dehydroxylation can begin at temperatures as low as 150 °C (Langer 2003), yet destruction of chrysotile and formation of forsterite occurs at much higher temperatures of 600–725 °C (Zaremba et al. 2010). It was described by Langer (2003) braking can result in ‘normal’ service temperatures of up to 650 °C but also ‘hot spots’ with temperatures well reaching as high as 1000 °C. However, the action of grinding is not the same as that of braking. While not an in-depth study, the temperatures on the surface of the middle of the brake shoe collected seconds after a series of many swipes back and forth with an AAMCO arc grinder were approximately 55 °C. Overall, it was found that while grinding can cause the shoes get hot to the touch, it is not hot enough to burn bare skin (RJ Lee Personal communication). Based on the minimal heating and short duration, it is unlikely that grinding alone could cause significant heat modification of chrysotile contained within the brake pad and certainly not the formation of forsterite.

Amphibole contamination

The role of amphibole contamination of chrysotile in the risk of MM (the so-called ‘amphibole hypothesis’) is a hotly debated topic. The hypothesis hinges on the observation of significantly higher proportion of amphibole fibers in the lungs of MM suffers despite higher levels of exposure to chrysotile (Roggli et al. 2002). Furthermore, study of MM incidence in Canadian chrysotile mines and mills where there is a <1% contamination of tremolite found the relative ratio of tremolite to chrysotile fibers in the lungs of workers is directly related to their risk (Mossman et al. 1990). Amphiboles are widely considered to be much more potent at causing MM than chrysotile (Berman and Crump 2008; Hodgson and Darnton 2010). As such, where amphiboles are present as a contaminating element of chrysotile, the overall MM generating potency of the mixed exposure would likely increase. Conversely, an absence of amphiboles would suggest a reduced potency (although we do not suggest removed), thus requiring heavy exposure to generate a significant risk of MM.

Electron microscopy analysis of the BD used within this study have shown no evidence of contaminating amphiboles. Furthermore, in the study by Bernstein and colleagues, their

analysis of BD described the BD generated by RJ Lee as containing no amphiboles in any of the aerosol or lung samples used in their study (Bernstein et al. 2015). Therefore, the overall potency of the BD in relation to MM would be considered to be significantly lower than if amphiboles were present given the relative potency of the two asbestiform minerals.

Macrophage brake debris interactions

The morphological and physicochemical characteristics of a particulate can tell us much about the potential nature of interactions with the cells tasked with clearing particulates from the lung. However, the true nature of interactions such as toxicity, and uptake can only be truly shown with *in vitro* or *in vivo* analysis. A pilot level assessment of cytotoxicity and phagocytosis were conducted and demonstrated that across a wide dose range, pure chrysotile asbestos was significantly more cytotoxic than BD. This is perhaps unsurprising if we consider the matrix fragments (resin containing carbon and iron particles) as being a relatively low toxicity material and the chrysotile within the BD as being the more biologically active sub-fraction.

A key aspect of the FPP is the impact shape (length) can have on particle clearance and toxicity. As demonstrated most recently by Schinwald et al. (2012), fibers >5 µm can impair macrophage mobility (and hence clearance rate) while longer fibers would provide troublesome to internalize and fibers with a cutoff length of 14 µm caused fiber induced pulmonary inflammation. The interaction between macrophages and fibers therefore is of great interest.

Where particles and fibers are encountered, macrophages will attempt to phagocytose and in the case of those particulates that are sufficiently small, these will be fully internalized (as demonstrated by the TEM analysis). However, as shown for both the chrysotile and BD test materials, where long fibers are present, attempted internalization will fail resulting in fiber(s) protruding from the cellular membrane. What this shows is that irrespective of the sample, if long fibers are present they will likely cause long fiber effects (in this case, frustrated phagocytosis). The key difference between the UICC-Chry-B sample and the BD is the proportion of long fibers (i.e. the long fiber dose). As described in lung deposition analysis, around 11% of the BD within an aerosol would likely deposit in the alveolar region and of that 11%, 15–17% of the total entities analyzed were >5µm in length. Therefore, on an equal mass exposure basis, a BD containing aerosol contains a far lower long fiber dose than the equivalent exposure to pure chrysotile. This is, in part demonstrated by the observation of a far greater proportion of THP-1 cells showing incomplete fiber uptake (38.1%) after treatment with chrysotile than the BD-treated cells which showed fibers protruding from the surface 0.8–1.8% of scored cells.

Conclusions

Together with dose, physicochemical properties of a particulate are key factors in determining pathogenicity. As shown, BD from chrysotile containing brake pads are highly heterogeneous in morphology and consist of around 17% of free chrysotile fibers with the fraction of the total aerosol that could penetrate the alveolar region of the lung. The average length of these fibers is cause for concern in relation to a fiber-type hazard and this is supported by the pilot macrophage study showing that where long fibers are present (either within the pure chrysotile or as a sub-fraction of the BD samples), incomplete uptake akin to frustrated phagocytosis is observed.

However, an important component of the FPP is the bio-persistence of fibers which is influenced by both length (in relation to cell mediated clearance) and chemical durability. Acellular assessment of biodurability indicate a pattern of rapid dissolution over a period of 14 days that is consistent across both chrysotile containing BD and pure chrysotile. Ultimately, the dissolution in a static system led to a complete destruction of fiber morphology with very little evidence of either free respirable fibers or non-WHO fibers being present after 84-days incubation in ALF. Such rapid dissolution and loss of fibers within chrysotile containing samples is in contrast to the durable amphibole, amosite which in turn fits with the higher levels of lung retention of amphiboles within the lung (Rasmuson et al. 2014). Overall, this characterization study indicates that long free chrysotile fibers are presented in BD and are respirable yet are of relatively low bio-durability and incubation in a low pH artificial lysosomal environment leads to a destruction of the free fibers present.

Acknowledgments

The authors wish to thank Dr. Sofia Billett and Mr. Steve Clark for their expertise in SEM analysis and Ms. Gillian Carse and Ms. Carolyn McGonagle for their expertise in gravimetric and elemental analysis. The authors also wish to acknowledge funding from Honeywell International Inc. and Ford Motor Company.

Author contributions

Matthew S. P. Boyles and Craig A. Poland contributed equally to this work.

Disclosure statement

Concept Life Sciences and IOM Consulting undertake independent consulting activities for private companies, regulators and government agencies. The sponsors and their representatives' roles were limited to providing study funding; they have had no input into the design/interpretation of the study or development of the paper. Neither the sponsors nor any of their in-house or outside legal counsel reviewed the paper prior to publication. The authors have not appeared in any regulatory or legal proceedings related to the content of this paper. The content and conclusions presented are the professional work of the authors and as such, may not represent the views of the sponsor or their employees. Honeywell and Ford are defendants in asbestos-product litigation involving automotive brakes.

Funding

This work was funded by Honeywell International Inc. and Ford Motor Company.

References

- Andreozzi GB, Pacella A, Corazzari I, Tomatis M, Turci F. 2017. Surface reactivity of amphibole asbestos: a comparison between crocidolite and tremolite. *Sci Rep.* 7(1):14696.
- Anjilvel S, Asgharian B. 1995. A multiple-path model of particle deposition in the rat lung. *Fund Appl Toxicol.* 28(1):41–50.
- Becklake MR, Bagatin E, Neder JA. 2007. Asbestos-related diseases of the lungs and pleura: uses, trends and management over the last century. *Int J Tuberc Lung Dis.* 11(4):356–369.
- Berman DW, Crump KS. 2008. A meta-analysis of asbestos-related cancer risk that addresses fiber size and mineral type [Meta-Analysis Research Support, Non-U.S. Gov't Research Support, U.S. Gov't, Non-P.H.S.]. *Crit Rev Toxicol.* 38(sup1):49–73.
- Bernstein DM, Chevalier J, Smith P. 2005. Comparison of Calidria chrysotile asbestos to pure tremolite: final results of the inhalation biopersistence and histopathology examination following short-term exposure. *Inhal Toxicol.* 17(9):427–449.
- Bernstein DM, Riego Sintes JM. 1999. Methods for the determination of the hazardous properties for human health of man made mineral fibres (MMMMF). EUR18748 EN. European Commission Joint Research Centre, Institute for Health and Consumer Protection, Unit: Toxicology and Chemical Substances, European Chemicals Bureau.
- Bernstein DM, Rogers RA, Sepulveda R, Kunzendorf P, Bellmann B, Ernst H, Creutzenberg O, Phillips JL. 2015. Evaluation of the fate and pathological response in the lung and pleura of brake dust alone and in combination with added chrysotile compared to crocidolite asbestos following short-term inhalation exposure. *Toxicol Appl Pharmacol.* 283(1):20–34.
- Bernstein DM, Rogers R, Sepulveda R, Kunzendorf P, Bellmann B, Ernst H, Phillips JL. 2014. Evaluation of the deposition, translocation and pathological response of brake dust with and without added chrysotile in comparison to crocidolite asbestos following short-term inhalation: interim results. *Toxicol Appl Pharmacol.* 276(1): 28–46.
- Bernstein D, Rogers R, Smith P. 2005. The biopersistence of Canadian chrysotile asbestos following inhalation: final results through 1 year after cessation of exposure. *Inhal Toxicol.* 17(1):1–14.
- Bernstein DM, Rogers R, Smith P. 2004. The biopersistence of Brazilian chrysotile asbestos following inhalation. *Inhal Toxicol.* 16(11-12):745–761.
- Braakhuis HM, Park MV, Gosens I, De Jong WH, Cassee FR. 2014. Physicochemical characteristics of nanomaterials that affect pulmonary inflammation. *Part Fibre Toxicol.* 11(1):18.
- Cho WS, Duffin R, Thielbeer F, Bradley M, Megson IL, Macnee W, Poland CA, Tran CL, Donaldson K. 2012. Zeta potential and solubility to toxic ions as mechanisms of lung inflammation caused by metal/metal-oxide nanoparticles. *Toxicol Sci.* 126(2):469–477.
- Coin PG, Roggli VL, Brody AR. 1992. Deposition, clearance, and translocation of chrysotile asbestos from peripheral and central regions of the rat lung. *Environ Res.* 58(1-2):97–116.
- Davis J, Addison J, Bolton R, Donaldson K, Jones A, Smith T. 1986. The pathogenicity of long versus short fibre samples of amosite asbestos administered to rats by inhalation and intraperitoneal injection. *Br J Exp Pathol.* 67(3):415–430.
- Ding Y, Stahlmecke B, Jiménez AS, Tuinman IL, Kaminski H, Kuhlbusch TAJ, van Tongeren M, Riediker M. 2015. Dustiness and deagglomeration testing: interlaboratory comparison of systems for nanoparticle powders. *Aerosol Sci Technol.* 49(12):1222–1231.
- Donaldson K, Murphy FA, Duffin R, Poland CA. 2010. Asbestos, carbon nanotubes and the pleural mesothelium: a review and the

- hypothesis regarding the role of long fibre retention in the parietal pleura, inflammation and mesothelioma. *Part Fibre Toxicol.* 7(1):5.
- Duffin R, Gilmour PS, Schins RP, Clouter A, Guy K, Brown DM, MacNee W, Borm PJ, Donaldson K, Stone V. 2001. Aluminium lactate treatment of DQ12 quartz inhibits its ability to cause inflammation, chemokine expression, and nuclear factor-kappaB activation [Research Support, Non-U.S. Gov't]. *Toxicol Appl Pharmacol.* 176(1):10–17.
- Egilman DS, Billings MA. 2005. Abuse of epidemiology: automobile manufacturers manufacture a defense to asbestos liability. *Int J Occup Environ Health.* 11(4):360–371.
- Finkelstein MM. 2015. Asbestos fibres in the lungs of an American mechanic who drilled, riveted, and ground brake linings: a case report and discussion. *Ann Occup Hyg.* 59(4):525–527.
- Finley BL, Richter RO, Mowat FS, Mlynarek S, Paustenbach DJ, Warmerdam JM, Sheehan PJ. 2007. Cumulative asbestos exposure for US automobile mechanics involved in brake repair (circa 1950s–2000). *J Expo Sci Environ Epidemiol.* 17(7):644–655.
- Fubini B. 1997. Surface reactivity in the pathogenic response to particulates. *Environ Health Perspect.* 105(Suppl 5):1013–1020.
- Garabrant DH, Alexander DD, Miller PE, Fryzek JP, Boffetta P, Teta MJ, Hessel PA, Craven VA, Kelsh MA, Goodman M. 2016. Mesothelioma among motor vehicle mechanics: an updated review and meta-analysis. *ANNHYG.* 60(8):1036–1026.
- Goodman M, Teta MJ, Hessel PA, Garabrant DH, Craven VA, Scrafford CG, Kelsh MA. 2004. Mesothelioma and lung cancer among motor vehicle mechanics: a meta-analysis. *Ann Occup Hyg.* 48(4):309–326.
- Grigoratos T, Martini G. 2015. Brake wear particle emissions: a review. *Environ Sci Pollut Res.* 22(4):2491–2504.
- Gualtieri AF. 2018. Towards a quantitative model to predict the toxicity/pathogenicity potential of mineral fibers. *Toxicol Appl Pharmacol.* 361:89.
- Gualtieri AF, Pollastri S, Bursi Gandolfi N, Gualtieri ML. 2018. In vitro acellular dissolution of mineral fibres: a comparative study. *Sci Rep.* 8(1):7071.
- Gualtieri AF, Tartaglia A. 2000. Thermal decomposition of asbestos and recycling in traditional ceramics. *J Eur Ceram Soc.* 20(9):1409–1418.
- Gualtieri AF, Viani A, Sgarbi G, Lusvardi G. 2012. In vitro biodurability of the product of thermal transformation of cement-asbestos. *J Hazard Mater.* 205–206:63–71.
- Gustavsson P, Plato N, Lidstrom EB, Hogstedt C. 1990. Lung cancer and exposure to diesel exhaust among bus garage workers. *Scand J Work Environ Health.* 16(5):348–354.
- Haka AS, Grosheva I, Chiang E, Buxbaum AR, Baird BA, Pierini LM, Maxfield FR. 2009. Macrophages create an acidic extracellular hydrolytic compartment to digest aggregated lipoproteins. *MBOC.* 20(23):4932–4940.
- Hatch D. 1970. Possible alternatives to asbestos as a friction material. *Ann Occup Hyg.* 13(1):25–29.
- Hesterberg TW, Anderson R, Bernstein DM, Bunn WB, Chase GA, Jankousky AL, Marsh GM, McClellan RO. 2012. Product stewardship and science: safe manufacture and use of fiber glass. *Regulatory toxicology and pharmacology.* RTP. 62(2):257–277.
- Hesterberg TW, Miiller WC, McConnell EE, Chevalier J, Hadley JG, Bernstein DM, Thevenaz P, Anderson R. 1993. Chronic inhalation toxicity of size-separated glass fibers in Fischer 344 rats. *Fundam Appl Toxicol.* 20(4):464–476.
- Hodgson JT, Darnton A. 2010. Mesothelioma risk from chrysotile. *Occup Environ Med.* 67(6):432.
- Kelsh MA, Craven VA, Teta MJ, Mowat FS, Goodman M. 2007. Mesothelioma in vehicle mechanics: is the risk different for Australians?. *Occup Med (Lond).* 57(8):581–589.
- Kim J, Chankeshwara SV, Thielbeer F, Jeong J, Donaldson K, Bradley M, Cho WS. 2016. Surface charge determines the lung inflammogenicity: a study with polystyrene nanoparticles. *Nanotoxicology.* 10(1):94–101.
- Laden F, Stampfer MJ, Walker AM. 2004. Lung cancer and mesothelioma among male automobile mechanics: a review. *Rev Environ Health.* 19(1):39–61.
- Langer AM. 2003. Reduction of the biological potential of chrysotile asbestos arising from conditions of service on brake pads. *Regulatory toxicology and pharmacology.* RTP. 38(1):71–77.
- Langer AM, McCaughey WT. 1982. Mesothelioma in a brake repair worker. *Lancet (London, England).* 2(8307):1101–1103.
- Li N, Xia T, Nel AE. 2008. The role of oxidative stress in ambient particulate matter-induced lung diseases and its implications in the toxicity of engineered nanoparticles. *Free Radical Biol Med.* 44(9):1689–1699.
- Light WG, Wei ET. 1977. Surface charge and asbestos toxicity [Research Support, U.S. Gov't, Non-P.H.S.]. *Nature.* 265(5594):537–539.
- Luoto K, Holopainen M, Kangas J, Kalliokoski P, Savolainen K. 1998. Dissolution of short and long rockwool and glasswool fibers by macrophages in flow through cell culture. *Environ Res.* 78(1):25–37.
- Lynch JR. 1968. Brake lining decomposition products. *J Air Poll Control Assoc.* 18(12):824–826.
- Committee on Hazardous Substances (AGS) 2014. TRGS 910 Risk-related concept of measures for activities involving carcinogenic hazardous substances. Dortmund, DE: Federal Institute for Occupational Safety and Health.
- Marques MR, Loebenberg R, Almukainzi M. 2011. Simulated biological fluids with possible application in dissolution testing. *Dissolution Technol.* 18(3):15–28.
- McConnell EE, Kamstrup O, Musselman R, Hesterberg TW, Chevalier J, Miiller WC, Thevenaz P. 1994. Chronic inhalation study of size-separated rock and slag wool insulation fibers in Fischer 344/n rats. *Inhal Toxicol.* 6(6):571–614.
- HSE 2005. EH 40/2005 workplace exposure limits. Sudbury (UK): HSE Books.
- IARC 2012. IARC monographs on the evaluation of carcinogenic risks to humans. Volume 100C: arsenic, metals, fibres and dusts. Lyon: IARC.
- ISO 2002. ISO 14966:2002: Ambient air – determination of numerical concentration of inorganic fibrous particles – scanning electron microscopy method. Geneva: International Organization for Standardization (ISO).
- Mossman BT, Bignon J, Corn M, Seaton A, Gee JB. 1990. Asbestos: scientific developments and implications for public policy. *Science.* 247(4940):294–301.
- Oberdorster G, Graham U. 2018. Predicting EMP hazard: lessons from studies with inhaled fibrous and non-fibrous nano- and micro-particles. *Toxicol Appl Pharmacol.* 361:50–61.
- Paustenbach DJ, Finley BL, Lu ET, Brorby GP, Sheehan PJ. 2004. Environmental and occupational health hazards associated with the presence of asbestos in brake linings and pads (1900 to present): a “state-of-the-art” review. *J Toxicol Environ Health Part B Crit Rev.* 7(1):25–80.
- Paustenbach DJ, Richter RO, Finley BL, Sheehan PJ. 2003. An evaluation of the historical exposures of mechanics to asbestos in brake dust. *Appl Occup Environ Hyg.* 18(10):786–804.
- Poland C, Duffin R. 2019. The toxicology of chrysotile-containing brake debris: implications for mesothelioma. *Crit Rev Toxicol.* 49(1):11–35.
- Poland CA, Schinwald A, Duffin R, Donaldson K, Cherrie JW. 2018. What makes a fibre, a fibre? The asbestos origins of the fibre length threshold and its verification with nanotechnology. *Occup Health.* 15(4):21–26.
- Price O, Asgharian B, Miller F, Cassee F, de Winter-Sorkina R. 2002. Multiple Path Particle Dosimetry model (MPPD v1.0): A model for human and rat airway particle dosimetry. RIVM rapport 650010030. Bilthoven: RIVM.
- Rasmuson JO, Roggli VL, Boelter FW, Rasmuson EJ, Redinger CF. 2014. Cumulative retrospective exposure assessment (REA) as a predictor of amphibole asbestos lung burden: validation procedures and results for industrial hygiene and pathology estimates. *Inhal Toxicol.* 26(1):1–13.
- Rodelsperger K, Jahn H, Bruckel B, Manke J, Paur R, Woiwitz HJ. 1986. Asbestos dust exposure during brake repair. *Am J Ind Med.* 10(1):63–72.

- Roggli VL, Vollmer RT, Butnor KJ, Sporn TA. 2002. Tremolite and mesothelioma. *Ann Occup Hyg.* 46(5):447–453.
- Rohl AN, Langer AM, Wolff MS, Weisman I. 1976. Asbestos exposure during brake lining maintenance and repair. *Environ Res.* 12(1):110–128.
- Salazar N, Cely-Garcia MF, Breyse PN, Ramos-Bonilla JP. 2015. Asbestos exposure among transmission mechanics in automotive repair shops. *Ann Occup Hyg.* 59(3):292–306.
- Schinwald A, Murphy FA, Prina-Mello A, Poland CA, Byrne F, Movia D, Glass JR, Dickerson JC, Schultz DA, Jeffree CE, et al. 2012. The threshold length for fiber-induced acute pleural inflammation: shedding light on the early events in asbestos-induced mesothelioma. *Toxicol Sci.* 128(2):461–470.
- Searl A. 1997. A comparative study of the clearance of respirable para-aramid, chrysotile and glass fibres from rat lungs. *Ann Occup Hyg.* 41(2):217–233.
- Searl A, Buchanan D, Cullen R, Jones A, Miller B, Soutar C. 1999. Biopersistence and durability of nine mineral fibre types in rat lungs over 12 months. *Ann Occup Hyg.* 43(3):143–153.
- Stanton MF, Layard M, Tegeris A, Miller E, May M, Kent E. 1977. Carcinogenicity of fibrous glass: pleural response in the rat in relation to fiber dimension. *J Natl Cancer Inst.* 58(3):587–603.
- Vallyathan V, Mega JF, Shi X, Dalal NS. 1992. Enhanced generation of free radicals from phagocytes induced by mineral dusts. *Am J Respir Cell Mol Biol.* 6(4):404–413.
- Van Orden DR. 1964. 2 – Asbestos. In: Morrison RD, Murphy BL, editors. *Environmental forensics*. Burlington: Academic Press; p. 19–33.
- Virta RL. 2002. Asbestos geology, mineralogy, mining, and uses. Version 1.0. Reston, VA: U.S. Department of the Interior, U.S. Geological Survey (US Geological Survey open-file report).
- Weir FW, Meraz LB. 2001. Morphological characteristics of asbestos fibers released during grinding and drilling of friction products. *Appl Occup Environ Hyg.* 16(12):1147–1149.
- WHO 1997. Determination of airborne fibre number concentrations. A recommended method, by phase-contrast optical microscopy membrane filter method. World Health Organization. <https://apps.who.int/iris/handle/10665/41904>
- Wong O. 2001. Malignant mesothelioma and asbestos exposure among auto mechanics: appraisal of scientific evidence. *Regulatory toxicology and pharmacology.* RTP. 34(2):170–177.
- Zaremba T, Krzakała A, Piotrowski J, Garczorz D. 2010. Study on the thermal decomposition of chrysotile asbestos. *J Therm Anal Calorim.* 101(2):479–485.